EXPERIMENTAL AND NUMERICAL STUDY OF THE NON-UNIFORM TOTAL TEMPERATURE IN A TURBULENT MACH 0.6 VORTEX STREET

W.P. Bennett* , A. Rona† , J.R. Ackerman‡ , J.P. Gostelow§
Department of Engineering
University of Leicester
Leicester LE1 7RH, UK

W.E. Carscallen¶
Gas Turbine Aerodynamics and Combustion Group
Institute for Aerospace Research
National Research Council of Canada
Ottawa, Ontario K1A 0R6, Canada

NOMENCLATURE

Symbols

c_p	Specific heat at constant pressure
M	Mach number
p	Pressure, kN/m^2
Re_D	Free stream Reynolds number
R	Specific gas constant, $287J/\left(kgK\right)$
s	Entropy, $J/\left(kgK\right)$
T	Temperature, K
t	Time, *sec.*
U	Velocity, m/s
x, y, z	Cartesian body axes, m
ρ	Density, kg/m^3
$\|\|$	Absolute value

Subscripts

s	Stagnation condition
∞	Free stream

ABSTRACT

This work investigates the non-uniform total temperature and total pressure downstream of a circular cylinder in transonic flow. At Mach 0.6 shock induced separation of the flow occurs from the surface of the cylinder. The unsteady shear layers roll up into vortices that are shed from the cylinder forming a von Kármán vortex street of convecting vortices. An experimental investigation of the vortex street is carried out at a distance of six cylinder diameters downstream. Time resolved total temperature measurements reveal the presence of localised 'hot spots' of increased total temperature at the edges of the wake and localised 'cold spots' of decreased total temperature along the centre of the wake. The experimental measurements are compared against a concurrent numerical study using a time accurate numerical model with turbulence closure. The numerical model also captures the non-uniform total temperature and total pressure distribution downstream of the cylinder. The non-uniform total temperature and total pressure distribution is shown to be a source of entropy production. Comparison of the total temperature and total pressure distribution highlights the influence of the boundary layer development and separation characteristics on the vortex shedding and energy separation processes. This emphasizes the importance of including the effects of turbulence and boundary layer development in numerical studies of the energy separation downstream of circular cylinders.

*Research Student.
†Lecturer.
‡Research Student.
§Professor.
¶Group Leader.

INTRODUCTION

Experimental and numerical studies of the non-uniform total temperature in the wake of a circular cylinder in a compressible Mach 0.6 flow are presented. At this Mach number, shock induced separation of the boundary layer forms a shear layer. The shear layer rolls up forming a vortex downstream of the cylinder. Vortices are shed alternately from each side of the cylinder, forming a von Kármán vortex street. This vortex shedding is responsible for the convection of the total enthalpy downstream of the cylinder giving a non-uniform total temperature distribution. Localised regions of increased total temperature above the freestream value, are present in the shear layer at the outer edge of the wake and localised regions of lower total temperature are present at the centre of the wake.

Eckert & Weise[1] first observed the time averaged non-uniform total temperature distribution using an embedded thermocouple at the base of a cylinder. This

work has been substantiated through subsequent research, including the time averaged experimental work of Ryan,[2] Thomann[3] and the integrated experimental and numerical research of Kurosaka et al.[4]

The non-uniform total temperature distribution observed in the circular cylinder wake also occurs downstream of turbine blades with thick trailing edges. This non-uniform distribution promotes entropy production leading to a total pressure loss between stages, thereby reducing the turbine stage performance. The service life of turbine blades is also reduced by the presence of hot spots close to the surface of the blade. The non-uniform total temperature and pressure distribution downstream of turbine blades with thick trailing edges have been studied by Carscallen & Oosthuizen[5] and Carscallen et al.[6,7]

The present research is a fundamental investigation into the flow physics of the mechanism responsible for the generation of the non-uniform total temperature distribution. This includes the effects of compressibility on the energy separation mechanism. A time accurate numerical model has been developed to reproduce the essential physics of the compressible turbulent wake flow, which is dominated by von Kármán vortex shedding. To reproduce the large-scale instabilities, the short-time Reynolds Averaged Navier Stokes (RANS) equations are computed over the flow domain. In addition, results of a concurrent time accurate experimental program, performed at the National Research Council of Canada (NRC), are documented. The integration of the experimental and numerical approaches provides a powerful tool for developing an improved understanding of this phenomenon.

FLOW CONDITIONS

The unsteady transonic flow around a circular cylinder is studied using both experimental and numerical methods. The numerical model cylinder diameter differs from previous work[8,9] for dynamic similarity with the experimental program. A cold flow of Mach number $M = 0.6$ approaches the cylinder. The Reynolds number of the free stream flow Re_D is 6.875×10^5. This is based on a cylinder diameter of $D = 37.26 \times 10^{-3}\ m$ for the experiment and $D = 47.41 \times 10^{-3}\ m$ for the numerical model. A constant total pressure of $p_s = 156.8\ kN/m^2$ is maintained upstream of the cylinder in the experiment. An unheated blow down trisonic type wind tunnel is used for the experimental program. Blow down operation results in the free stream total temperature T_s dropping over the course of the experiment due to expansion of the air in the supply tanks. Perforated walls are employed in the test section to attenuate end wall interference effects. A uniform flow condition is defined at the inlet boundary for the numerical model. At the inlet boundary the density $\rho_\infty = 1.261\ kg/m^3$, the total pressure $p_s = 129.24\ kN/m^3$, the static pressure $p_\infty = 101.325\ kN/m^3$, the total temperature $T_s = 300\ K$, static temperature $T_\infty = 280\ K$ and velocity $U_\infty = 201.25\ m/s$. The free stream kinetic energy $k_\infty = 0.10\ m^2/s^2$ and the specific dissipation rate $\omega_\infty = 5221\ m/s^2$. This is equivalent to a turbulence intensity of approximately 0.13% and models a quiet wind tunnel. The free stream flow conditions used in the experiment and the numerical model are summarized in Table 1. Results from the experiment and the numerical prediction are presented in non-dimensional form. The mean free stream flow conditions are used to normalise the local flow variables, and the parameter D/U_∞ normalises time.

Parameter	Experiment	Numerical Model
M	0.6	0.6
Re_D	6.875×10^5	6.875×10^5
p_s	156.8 kN/m^2	129.24 kN/m^2
p_∞	122.9 kN/m^2	101.325 kN/m^2
$\frac{1}{2}\rho U_\infty^2$	31.0 kN/m^2	25.536 kN/m^2

Table 1 Free stream flow conditions

NUMERICAL MODEL

A turbulent numerical model solves the short-time averaged Navier-Stokes equations.[10] Turbulence closure is obtained using the two equation $k-\omega$ model of Wilcox.[11] An explicit, upwind cell centred method is employed. Second order formal accuracy in space is achieved through the use of the Monotone Upwind Scheme for Conservation Laws (MUSCL) interpolation technique to estimate the inviscid fluxes at each cell interface. For this study the approximate Riemann solver of Roe[12,13] is used. The two-step Runge-Kutta method of Hu et al.[14] is used for flux integration over the finite volume boundaries. Second order formal accuracy is achieved using the standard Runge-Kutta coefficients $(1.0, 0.5)$. A detailed description of the numerical model is given in previous work.[8,9] A $30.2D \times 25.3D$ rectangular computational domain is defined around the circular cylinder. This is given in Fig. 1. A non-uniform, structured mesh of rectangular topology forms the computational mesh. This mesh is body-fitted around the cylinder and proportional (linear) grid stretching is employed normal to the surface of the cylinder to obtain a fine discretization close to the cylinder surface. Four adjacent topologically orthogonal blocks are defined through multi-domain decomposition. These are illustrated in Fig. 1 using dashed lines to indicate inter-block boundaries. A computational mesh of 100×200 cells is defined inside each of the four adjacent blocks with a perimetrical frame of one cell depth for definition of boundary conditions and inter-block connectivity. This results

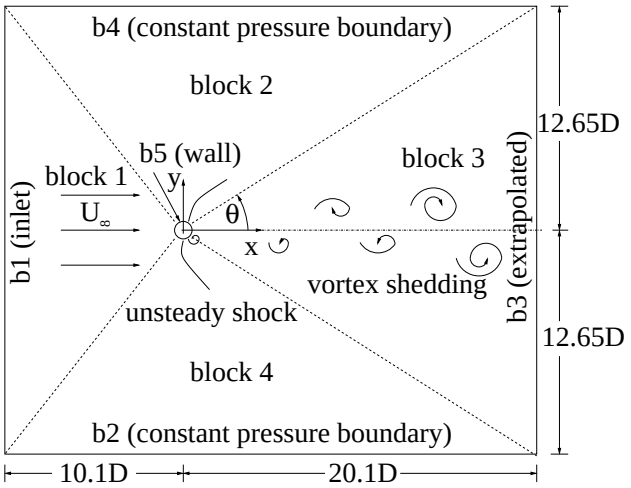

Fig. 1 Cylinder flow computational domain.

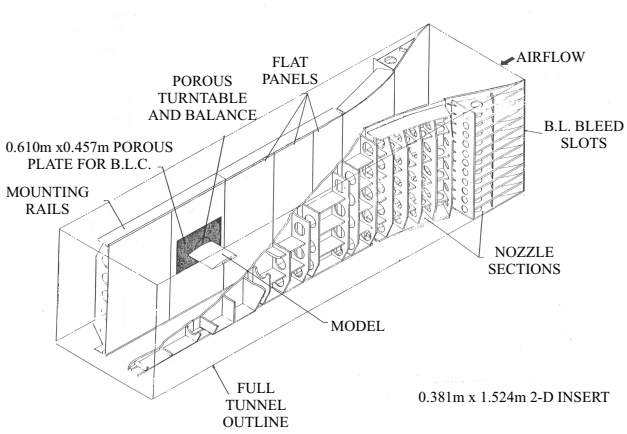

Fig. 2 Experimental Test Section.

in a total interior computational mesh of 400×200 cells. An elliptical grid generation scheme is used for the creation of the computational mesh. This employs a Gauss-Seidel method to reduce cell skewness by iteratively redistributing the grid points to generate a smoothly varying distribution of cell vertices.[15] This grid generation scheme results in a computational mesh with a unit cell aspect ratio of $1.226 \leq A \leq 6.43$, and cell size $(\Delta x, \Delta y)$ ranging from $(4.55 \times 10^{-3}D, 5.58 \times 10^{-3}D)$ to $(1.07D, 0.17D)$. A constant time step of $\Delta t = 0.001D/U_\infty$ is employed for the computational grid. The computational domain inlet boundary $b1$ is located at a distance of $10.1D$ upstream of the cylinder to allow decay of the pressure fluctuations travelling upstream. A subsonic inflow condition is enforced at this boundary based on the characteristic method of Giles.[16] A subsonic outlet condition is enforced at boundaries $b2$ and $b4$. These are located at a distance of $12.65D$ from the cylinder where the flow is almost parallel to the boundary. First order extrapolation of the interior conservative variables defines the outflow boundary condition, $b3$. This boundary is located at a distance of $20.1D$ downstream of the cylinder. An inviscid wall condition of zero normal velocity is imposed at the surface of the cylinder, $b5$.

At the start of the computation a uniform Mach 0.6 flow is imposed throughout the computational domain using the free stream conditions $(\rho_\infty, U_\infty, p_\infty, T_\infty)$. The numerical model is time marched from the initial uniform distribution to a quasi-stationary vortex shedding regime using the inviscid numerical method detailed in Rona & Bennett.[8] The development of the quasi-stationary vortex shedding inviscid flow prediction is detailed in Rona & Bennett.[8] The quasi-stationary inviscid flow prediction is then used to prime the turbulent computation. Free stream values for the short-time averaged kinetic energy production k_∞, and dissipation rate ω_∞ are defined throughout the computational domain. The turbulent flow field is then progressed to a quasi-stationary vortex shedding turbulent prediction. This method for the computation of the turbulent flow field is more computationally efficient with respect to solving the short-time averaged Navier-Stokes equations with $k - \omega$ turbulence closure from the initial uniform flow field. The quasi-stationary turbulent flow prediction using an inviscid wall condition at the cylinder surface is detailed in Rona & Bennett[9] for a free stream Reynolds number of $Re_D = 0.5 \times 10^6$, based on the cylinder diameter.

The numerical computation is performed on the University of Leicester Mathematical Modelling Centre's SGI Origin 2400 supercomputer, with 64 R14k, $500MHz$ processors and $32Gbytes$ RAM.

EXPERIMENTAL METHOD

A 1.5 metre trisonic blowdown wind tunnel with a two-dimensional (2-D) flow insert in the working section is used for the experimental part of this investigation. The schematic of the 2-D insert is shown in Fig. 2. The test section of the 2-D insert measures $0.381m \times 1.524m \times 3.581m$. The wind tunnel is run at constant Reynolds number and can be operated over a discharge Mach number range of 0.1 to 0.9, set by the total to static pressure ratio. Blowdown operation results in the free stream total temperature dropping over the course of each run as the air in the supply tanks expands. The model is mounted $2.388m$ downstream of the end of the nozzle on reinforced mounts. Boundary layer control is supplied using ejector-augmented sidewall suction through $0.610m \times 0.452m$ porous plates, Fig. 2. The balance can be rotated through a range of $\pm 55°$ at a rate of $15°$ per second. A single Kulite XCQ-062-25D ultraminiature pressure transducer is mounted so that the B-screen, which covers the pressure sen-

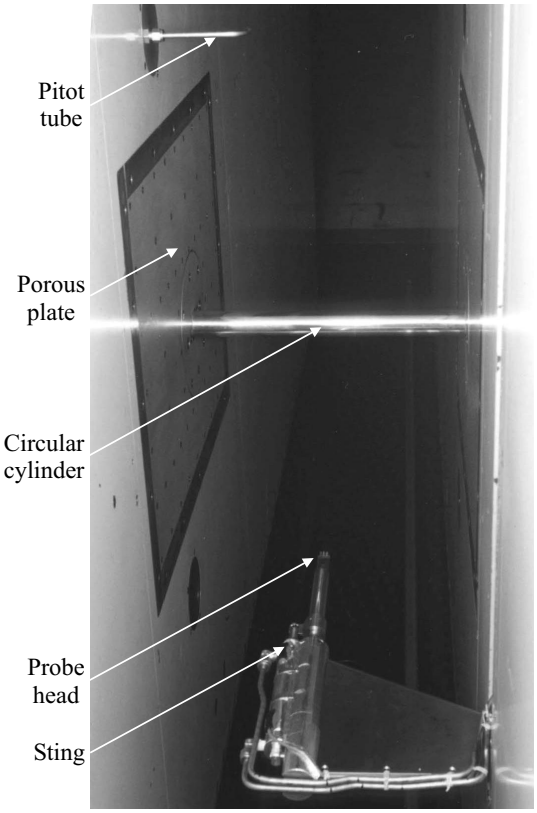

Fig. 3 Cylinder Wake Probe.

sitive diaphragm, is flush with the cylinder surface at midspan. The wake probe used for the traverse downstream of the cylinder consists of a total temperature transducer, developed at Oxford University, alongside a tube mounted Kulite XCQ-062-25D ultra-miniature pressure transducer. These are mounted in a green glass holder, attached to the end of a stainless steel tube. The Kulite pressure transducer is mounted with its face directly pointing into the flow, allowing the total pressure to be measured. The probes are mounted so that their tips are aligned along the horizontal spanwise axis of the wind tunnel. As the vortex shedding is assumed to be two-dimensional, mounting the probes in this way ensures simultaneous measurement of the total temperature and total pressure. The sting is mounted onto the wake traverse by way of a triangulated support. The sting and support are designed so that the probe tips are six cylinder diameters downstream of the model's leeward most point, Fig. 3. Measurement of total temperature is taken using the transducer developed at Oxford University by Buttsworth and Jones.[17] The transducer consists of two probes. Each total temperature probe is a $3mm$ diameter rod of fused quartz, one end of which is hemispherical. The hemispherical tips of both probes are painted with a platinum thin film resistance thermometer. Leads of gold paste are painted along the sides from the ends of the platinum thin films to the end of the probe to act as contacts for wiring.

Buttsworth and Jones[17] describe the measuring technique for the total temperature probes in detail, therefore, only a brief description is included here. The heat transfer between the quartz probe and the flow is governed by the heat transfer coefficient, the surface temperature of the quartz and the total temperature of the flow at the stagnation point. The thin film gauges are run in constant current mode so that the surface temperature of the quartz can be deduced from the voltage drop across the gauge. A high frequency heat transfer signal is generated from the gauge voltage via the heat transfer analogue in Oldfield et al.[18] Since both probes are nominally identical they are assumed to have the same heat transfer coefficient. Therefore, by heating one of the probes with a small internal heater prior to each measurement, so that the two probes have different surface temperatures, it is possible to simultaneously solve the heat transfer equation for both probes and calculate the flow total temperature. Corrections are applied for surface curvature effects and lateral conductions as described by Buttsworth and Jones.[17] Error analysis carried out by Buttsworth and Jones shows that the probe is capable of a measurement accuracy of $\pm 3K$. The frequency response of the thin film probes is limited by the conditioning electronics of the heat transfer analogue to $87kHz$. The total temperature probe was originally designed for use in transient wind tunnels. Since run times of exceeding two minutes are expected a novel way of using the probe has been developed. To this end an open-ended sheath that moves forward over the probe head during heating to provide an enclosure of stagnant air is mounted onto the sting. Also, while the probe is heated, the wind tunnel control valve is closed and the probe is traversed to $y/D = 3.22$ below the tunnel centre line. By doing this the free stream Mach number is reduced to between 0.1 and 0.15 and the probe is moved out of the fluctuating wake flow. Once the heated probe reaches $393K$ the heater is switched off, the control valve opened, the probe traversed into position and data acquisition started. After 0.2 seconds of data collection the sheath is withdrawn, opening the probe to the flow. Data collection then continues for a further 1.8 seconds. The traverse across the wake is conducted from a flow normal distance of $y = 3.22D$ above the wake to $y = 3.54D$ below the wake in steps of $y = 8 \times 10^{-2}D$. A simultaneous reading is taken from the Kulite pressure transducer in the cylinder with each wake measurement to act as a phase reference. For this purpose the cylinder is rotated so that the cylinder transducer is positioned 120° from the leading edge. This position for the phase reference is chosen because pressure mea-

surements made during a surface pressure survey have shown strong fluctuations at this location at the fundamental frequency of the vortex shedding. The signals are subjected to a $40kHz$ low-pass anti-aliasing filter before being recorded directly onto PC through National Instruments data acquisition cards at a sample rate of $100kHz$. Calibration procedures are applied to the data to produce of total temperature and total pressure signals in physical units. After filtering to remove noise and harmonic content, ensemble averaging is carried out on the data using the phase reference signals. The ensembles comprise of 64 blocks of eight cycles. The large number of blocks are necessary to remove noise from the signals; unfortunately it also results in removing much of the harmonic content resulting in almost sinusoidal signals, Fig. 4. To ensure that no data taken prior to the sheath being withdrawn or during flow establishment are included in the ensemble averaging, the first 0.3 seconds of data for each record are discarded. The use of a common phase reference transducer for the wake data and a similar common phase reference for the cylinder surface data enables the data to be combined into the contour plots in Figures $5(a)$, $6(a)$ and $7(a)$.

RESULTS & DISCUSSION

The numerical model is advanced to a computational time of $t = 183D/U_\infty$ from the onset of the turbulent computation ($t = 0$). An initial transient flow field develops immediately following the introduction of turbulence closure. At $t = 183D/U_\infty$ the surface pressure history indicates that a quasi stationary vortex shedding regime has resumed. In Figs. 5-7, a comparison of the numerical prediction with the results of the experimental test program is presented. These start at a computational time of $t = 183D/U_\infty$, which corresponds to $tU_\infty/D = 0$ in the time axis (abscissa) of Figures 5-7.

TOTAL TEMPERATURE FIELD

Figures $5(a)$ and $5(b)$ are contour plots of the total temperature distribution in the wake of the circular cylinder. The Eulerian frame of reference is used for the contour distribution. The ordinate in Figures $5(a, b)$ is the non dimensional flow normal distance from the centre of the wake ($y/D = 0$) on the $x = 6.5D$ plane, Fig. 1. The abscissa in Fig. 5 is the non dimensional time (tU_∞/D). The total temperature distribution in Figures $5(a, b)$ are both discretised over 10 contour levels for consistency between the experiment and computation. Figure $5(a)$ is the ensemble averaged total temperature distribution measured using the total temperature wake probe. Figure 5(b) shows contours of total temperature, computed using

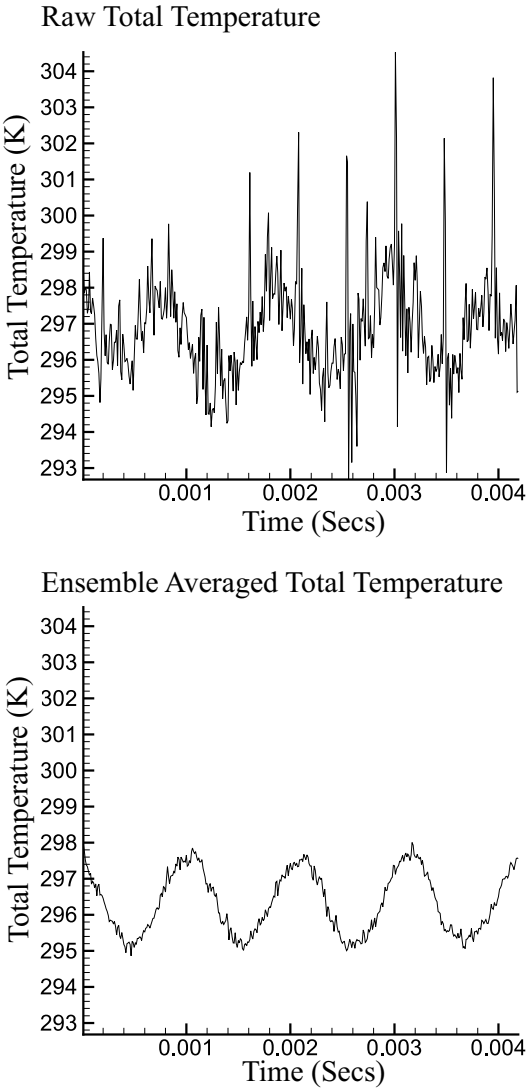

Fig. 4 Raw and Ensemble Averaged Data.

the numerical model. The total temperature is normalised using the free stream total temperature, $T_{s\infty}$. A dotted line is placed at $y/D = 0$. This denotes the position of the cylinder centre along the y/D (ordinate) axis normal to the flow. Vortices are shed from the surface of the cylinder in an alternating pattern. At six cylinder diameters downstream of the cylinder surface this pattern settles into a well defined von Kármán vortex street. The contours from the experimental measurement and numerical prediction both show a non uniform total temperature distribution in the von Kármán vortex street. Localised 'hot spots' of higher total temperature are present in the shear layer at the edge of the wake and localised 'cold spots' of lower total temperature are present at the centre of the wake. The mean location of the hot and cold spots relative to the centre of the wake can be determined from Figs. $5(a, b)$. The upper row of hot spots in

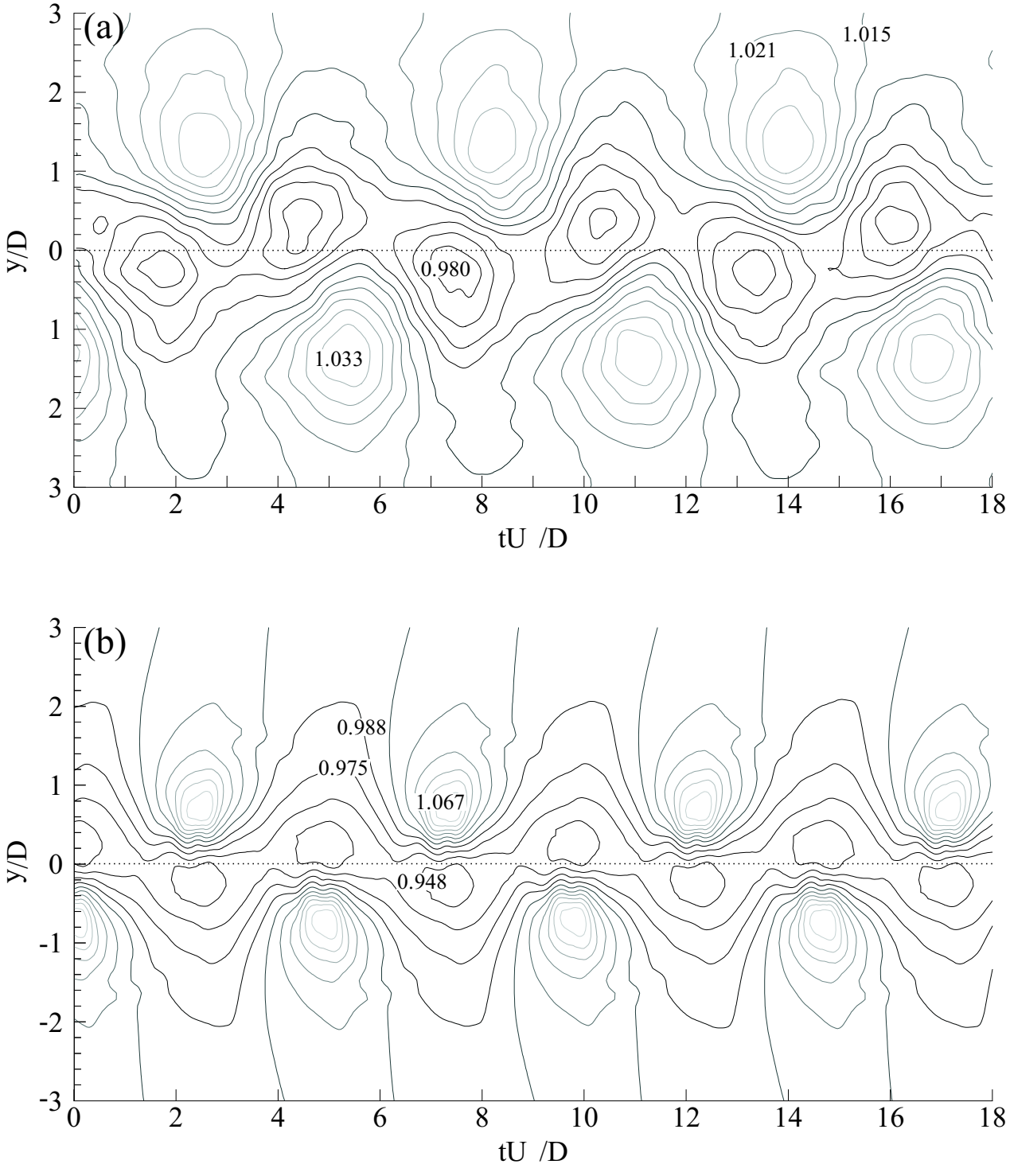

Fig. 5 Total temperature contours. (a) **Experiment** $\Delta T_s = 0.006 T_{s\infty}$, (b) **Prediction** $\Delta T_s = 0.013 T_{s\infty}$.

the measured total temperature distribution, Fig. 5(a) are centred at an average flow normal distance of approximately $\overline{y}_{T_{max}}/D = 1.3$, from the wake centreline. The lower row of hot spots are centred at approximately $\overline{y}_{T_{max}}/D = -1.3$. The measured cold spots are centred at an average distance of $\overline{y}_{T_{min}}/D = \pm 0.3$. The presence of hot and cold spots in the wake can be explained by extending the explanation put forward by Kurosaka et al.[4] for the total temperature non uniformity in incompressible flow. Each convecting vortex core is associated with a localised total temperature maximum (hot spot) and minimum (cold spot). In Figure 5(a), the upper row of vortices in the von Kármán vortex street are associated with the hot spots located at $\overline{y}_{T_{max}}/D = 1.3$, and the cold spots located at $\overline{y}_{T_{min}}/D = -0.3$. Similarly, the lower row of vortices are associated with the hot spots located at $\overline{y}_{T_{max}}/D = -1.3$ and the cold spots located at $\overline{y}_{T_{min}}/D = 0.3$. The maximum total temperature contour level in the measured distribution of Fig. 5(a) is $T_{max} = 1.033T_{s\infty}$. The corresponding measured total temperature minima is $T_{min} = 0.980T_{s\infty}$. Assuming a mean free stream total temperature of $T_{s\infty} = 293K$, these values correspond to a total temperature increase of $(T_{max} - T_{s\infty}) = 9.67K$ in the labelled hot spot at the edge of the wake with respect to the free stream flow, and a total temperature decrease of $(T_{s\infty} - T_{min}) = 5.86K$ in the labelled cold spot at the centre of the wake. A similar non-uniform total temperature distribution is noted in the predicted results, Fig. 5(b). The total temperature maxima in the numerical prediction of Figure 5(b) are centred at an average flow normal distance of approximately $\overline{y}_{T_{max}}/D = \pm 0.7$ for the upper and lower rows respectively. The total temperature minima in Fig. 5(b) are centred at an average flow normal distance of approximately $\overline{y}_{T_{min}}/D = \pm 0.2$. The corresponding magnitudes of total temperature maximum and minimum for the numerical prediction are $T_{max} = 1.067T_{s\infty}$ and $T_{min} = 0.948T_{s\infty}$. At the same free stream total temperature of $T_{s\infty} = 293K$ used in the experiment the total temperature increase in the labelled hot spot of Fig. 5(b) corresponds to an increase of $(T_{max} - T_{s\infty}) = 19.63K$ above the free stream total temperature. The decrease in total temperature in the labelled cold spot is $(T_{s\infty} - T_{min}) = 15.24K$ below the free stream total temperature. The magnitude and location of the hot and cold spots in Figs. 5(a, b) are summarised in Table 2. Comparing Figures 5(a) and 5(b), it is evident that the flow normal distance between the upper and lower row of hot spots is greater in the measured results. The measured increase in total temperature at the hot spots and the measured decrease in total temperature at the cold spots is also lower in magnitude than the predicted results. A difference in the temporal spacing of the hot spots is also noted between the experimental and numerical results. The adjacent hot spots (and cold spots) are more closely spaced along the abscissa in the numerical prediction. The variation in magnitude and location of the total temperature distribution is linked to different vortex shedding characteristics between the experiment and computation. This link between the non-uniform total temperature field and the vortex shedding characteristics is indicated in previous work for circular cylinders[4,8,9] and turbine blades.[6,7] To understand the variation in temporal spacing of the hot spots between the experimental and numerical results the respective vortex shedding frequencies are considered. The Strouhal number ($Str = fD/U_\infty$) is a non dimensional measure of the frequency (f) of vortex shedding in the wake of the circular cylinder. The Strouhal number in the experiment is $Str_{exp} = 0.176$. This is determined by performing a fast Fourier transform on the pressure measurements from the phase reference pressure transducer positioned on the cylinder surface at 120° from the leading edge. The Strouhal number in the numerical prediction is $Str_{num} = 0.204$. This is calculated using the average timewise spacing between successive vortices in the cylinder wake. The difference between the two predictions is approximately 14%. This represents a significant difference in the shedding frequency. A primary factor in the difference between the measured and predicted Strouhal numbers is the difference in flow conditions at the cylinder surface. The numerical model uses an inviscid wall condition at the cylinder surface, therefore, no boundary layer develops. The presence of the boundary layer on the cylinder surface increases the effective circular cylinder diameter from which vortices are shed in the equivalent inviscid model flow. This can be accounted for by normalising the experimental vortex shedding frequency (f) with respect to the cylinder diameter adjusted by the wall displacement thickness $\delta^\star$. The time averaged displacement thickness of the boundary layer at the time mean separation point on the cylinder is calculated from experimental boundary layer measurements in which a flattened pitot tube is used. An effective cylinder diameter D_e is defined as $(D_e = D + 2\delta^\star)$. Normalising the experimental data by D_e gives $Str_{exp} = fD_e/U_\infty = 0.189$. The agreement in Strouhal number with the numerical prediction therefore increases to approximately 7%. Consid-

Parameter	Experiment	Computation
Str	0.176	0.204
$T_{max}/T_{s\infty}$	1.033	1.067
$T_{min}/T_{s\infty}$	0.980	0.948
$\lvert\overline{y}_{T_{max}}/D\rvert$	1.3	0.7
$\lvert\overline{y}_{T_{min}}/D\rvert$	0.3	0.2

Table 2 Wake total temperature comparison

ering the boundary layer displacement thickness alone does not however account for the different boundary layer separation and reattachment characteristics with respect to the inviscid wall model flow dynamics. The broad agreement of the measured Strouhal number with the predicted Strouhal number computed using the numerical model without boundary layer development highlights the dominance of the inertial forces and compressibility effects over viscous effects at the current transonic free stream Mach number. The Mach 0.6 cylinder flow features shock induced flow separation at the surface of the cylinder that may serve to increase the agreement between the measured and predicted Strouhal numbers. The spacing between adjacent hot and cold spots in Figs. $5(a,b)$ matches the vortex spacing calculated from the Strouhal numbers indicating the presence of a hot spot and a cold spot around each convecting vortex core. The measured and predicted Strouhal numbers are summarised in Table 2. The different flow separation characteristics from the surface of the cylinder is responsible for tighter rolling up of vortices shed from the cylinder surface in the numerical model. This leads to closer spacing of the hot and cold spots, together with higher total temperatures at the hot spots and lower total temperatures at the cold spots. The influence of the vortex shedding on the magnitude and location of total temperature separation is also noted in the work of Carscallen et al.[6] in which asymmetric vortex shedding is observed downstream of a turbine blade in transonic flow. In the current numerical prediction the total temperature maxima and minima are aligned in pairs normal to the streamwise direction. This alignment of the maxima and minima was observed in the inviscid and turbulent prediction of previous work.[8,9] In the measured total temperature distribution, however, the cold region is shown to lead the hot spot on the time axis. This corresponds to a downstream location of the cold spot relative to the hot spot. This may be a result of the boundary layer separation and reattachment characteristics that are not modelled in this work. The difference in alignment of the hot and cold spots between the experiment and computation may eventually be accounted for through consideration of a numerical model with boundary layer development on the surface of the cylinder.

TOTAL PRESSURE FIELD

The total pressure distribution corresponding to Figures $5(a,b)$ are given in Figures $6(a,b)$. Figure $6(a)$ shows the ensemble averaged total pressure distribution measured using the Kulite XCQ-062-25D ultra-miniature pressure transducer. This is compared with the numerical prediction of Fig. $6(b)$. A dotted line is placed at $y/D = 0$ to denote the flow normal position of the cylinder centre. Significant differences are noted between the measured field and the numerical prediction. The total pressure distribution in the numerical prediction, Fig. $6(b)$, appears to follow the same pattern observed in the total temperature distribution of Fig. $5(b)$. Specifically, regions of total pressure higher than the free stream $p_{s\infty}$ are present at the outer edges of the wake, rising to a maximum value of $p_s = 1.089p_{s\infty}$ at an average flow normal distance of approximately $\overline{y}_{p_{max}}/D = \pm 1.1$ from the wake centreline for the upper and lower vortex rows respectively. Localised regions of lower total pressure are observed at the centre of the wake in the numerical prediction. The value of total pressure in these regions is approximately $p_s = 0.628p_{s\infty}$ at an average flow normal distance of $\overline{y}_{p_{min}}/D = \pm 0.2$ from the wake centreline, for the respective upper and lower vortex rows. The computed total pressure maxima and minima are aligned in pairs at the same x/D position downstream of the cylinder, similar to the observed pattern in the total temperature distribution. The total pressure maxima and minima are located further from the wake centreline than the corresponding total temperature hot and cold spots in Fig. $5(b)$. In the work of Kurosaka et al.[4] the computed total pressure distribution in the wake of the cylinder in incompressible flow is shown to be identical to the normalised total temperature distribution. The values for the normalised total pressure given in Kurosaka et al.[4] are equivalent to the normalised total temperature multiplied by a scaling factor of $\gamma/(\gamma - 1)$. In deriving this relationship Kurosaka et al.[4] assumed a constant density. At the Mach number used in the present work the compressibility of the fluid results in the observed shift in flow normal position of the total pressure maxima and minima in Figure $6(b)$ with respect to the total temperature in Figure $5(b)$.

The minimum total pressure in the measured results of Figure $6(a)$ is $p_s = 0.581p_{s\infty}$, this total pressure minimum is located within $y/D = \pm 0.2$ of the wake centreline. This compares to a predicted minimum total pressure of $p_s = 0.628p_{s\infty}$. Profile losses in the measured results due to the presence of the boundary layer account for the lower total pressure minimum compared with the numerical prediction. Periodicity in the measured total pressure minima is noted in Figure $6(a)$. The temporal spacing of the measured total pressure minima along the abscissa matches the time spacing between each vortex core. This indicates an association of each total pressure minima with a convecting vortex. The labelled total pressure maximum in Figure $6(a)$ remains below the free stream value. This is in contrast to the predicted results that show an increase in the total pressure above the free stream value at the edges of the wake. The increase in to-

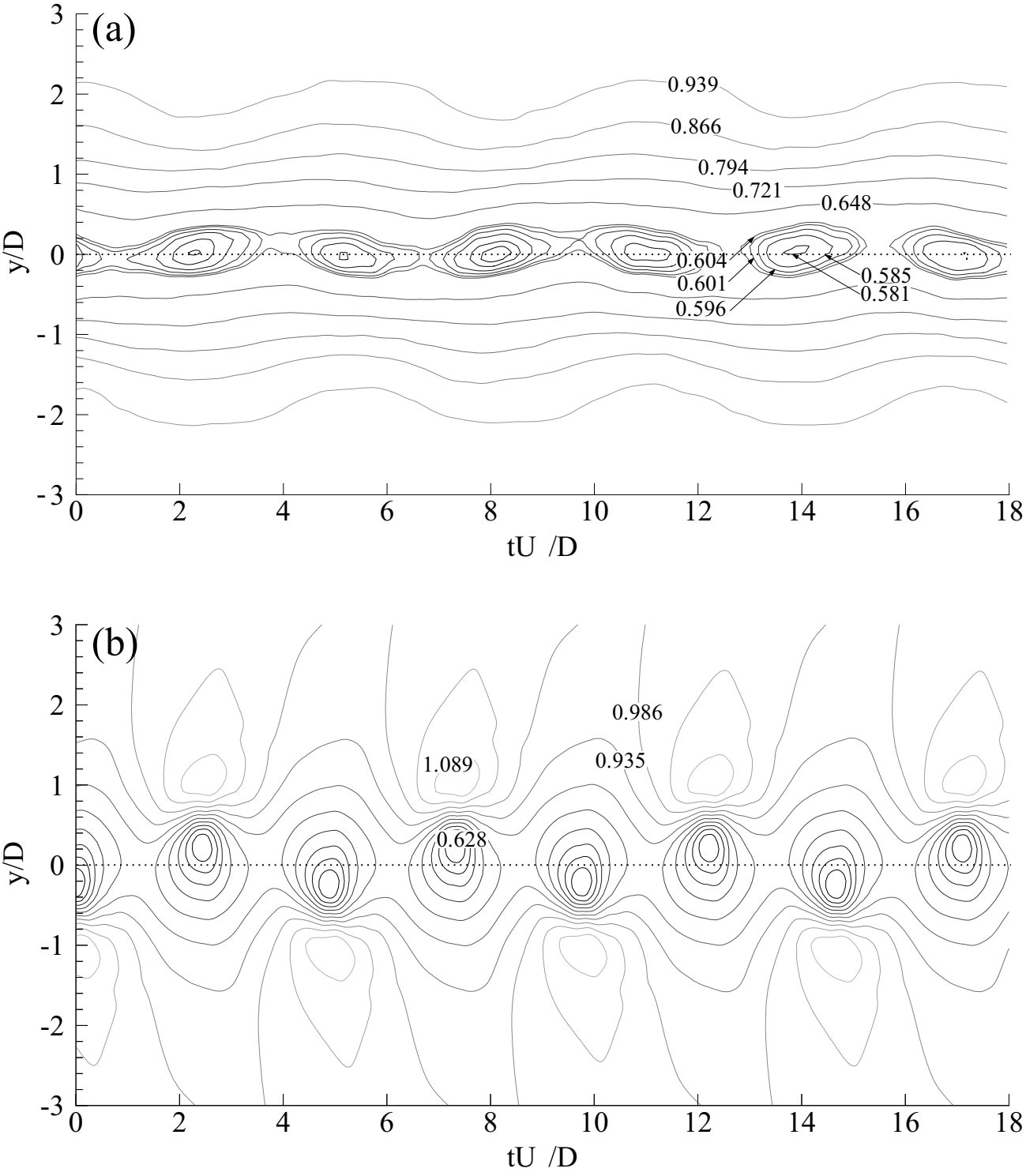

Fig. 6 Normalised total pressure contours. (a) **Experiment,** (b) **Numerical prediction.** $\Delta p_s = 0.051 p_{s\infty}$.

tal pressure above the free stream value was explained in Kurosaka et al.[4] as an exchange in work between two hypothetical fluid particles travelling a trochoidal pathline around a convecting vortex core. The particle travelling downstream of the convecting vortex core decreases in total temperature and total pressure due to the approaching low pressure vortex core. A similar fluid particle travelling upstream of the vortex core increases in total temperature and total pressure due to the receding low pressure vortex core. In this manner the convecting vortex acts to effectively exchange work between the two fluid particles. This exchange in work allows an increase of the total pressure along the outer edges of the wake. The contour spacing in the region of the predicted total pressure maximum and minimum indicates a significantly greater gradient at the total pressure minimum. The decrease in total pressure from the free stream value to the minimum total pressure contour is also significantly greater than the increase from the free stream to the total pressure maximum. The low increase in total pressure at the edge of the wake, spread over a larger region, may contribute to the lack of a significant measured total pressure increase above the free stream condition at the edges of the wake in the experimental results.

ENTROPY DISTRIBUTION

The total pressure and total temperature can be combined to give an account of the entropy production in the cylinder wake. The entropy increase over the free stream condition is calculated using Eqn. 1.

$$s = c_p \ln\left(\frac{T_s}{T_{s\infty}}\right) - R \ln\left(\frac{p_s}{p_{s\infty}}\right) \qquad (1)$$

where T_s is the local total temperature and p_s is the local total pressure. Entropy is a measure of the inability of the total temperature to respond to changes in the total pressure within the unsteady wake flow. The entropy distribution, calculated using the measured and predicted total temperature and total pressure fields at a downstream distance of six cylinder diameters is given in Figs. $7(a, b)$. The contours of entropy increase are normalised using $s_s = p_s/(\rho_s T_s) = 287J/(kgK)$. Figure $7(a)$ is a contour plot of the entropy increase, calculated using the measured total temperature and total pressure of Figs. $5(a)$ and $6(a)$. This is compared against the predicted entropy increase of Figure $7(b)$, calculated from the predicted total temperature and total pressure given in Figs. $5(b)$ and $6(b)$.

In Figure $7(a)$ regions of high entropy increase are located at flow normal positions close to the centre of the wake. These are periodically situated each side of the centre line at an average distance of $\overline{y}_{s_{max}}/D = 0.254$ for the upper row and $\overline{y}_{s_{max}}/D = -0.258$ for the lower row. The temporal spacing between entropy maxima matches the time period between successive vortices given by the Strouhal number. The measured entropy decreases with lateral distance towards the edges of the wake. The maximum labelled entropy level is $s_{max} = 0.525$. Comparing the measured results against the numerical prediction of Figure $7(b)$ it is evident that the predicted entropy maxima lie at a greater flow normal distance from the centre of the wake at $\overline{y}_{s_{max}}/D = \pm 0.376$. The predicted maximum entropy level is $s_{max} = 0.466$. The greater maximum entropy increase in the measured results follows the greater total pressure deficit observed at the centre of the wake in Figure $6(a)$ due in part to profile loss.

The entropy distribution is used to locate the centre of the convecting vortices. These are identified as regions of entropy maximum. As previously noted the flow normal distance between entropy maxima is lower for the measured results. This would appear contrary to the identified greater flow normal spacing between hot spots in Figure $5(a)$ and the lower vortex shedding frequency in the measured results. The geometry of the vortex street can be assessed through the vortex shedding aspect ratio, that is, the ratio of the flow normal distance (h) between the vortex rows to the streamwise spatial distance (l) between successive vortices of the same row. The spatial distance between successive vortices can be measured in the numerical prediction through the use of Lagrangian contours. These are taken from a frame of reference in which the cylinder is stationary. Inspection of the predicted Lagrangian entropy contours reveals a vortex shedding aspect ratio h/l of 0.276. This agrees well with the analytical model flow by von Kármán of $h/l = 0.281$ which typifies the von Kármán vortex street, as reported in Douglas et al.[19] As the flow normal distance (h) is lower in the measured results this would indicate a lower streamwise distance (l) between successive vortices for a similar aspect ratio. This is however contrary to the observed greater flow normal distance between hot spots in the total temperature distribution of Figure $5(a)$. The normalised total pressure field is the dominant influence in the entropy distribution close to the wake centreline. The lower flow normal distance in the measured results may therefore largely be a result of the greater total pressure deficit at the centre of the wake. The influence of the profile loss on the entropy distribution will eventually be addressed through comparison with a numerical model accounting for boundary layer development. A further source of entropy production can be identified from the predicted entropy distribution of Figure $7(b)$. Entropy is produced at the outer edges of the wake due to shearing of the flow between successive contra-rotating vortices. This source of entropy production has been shown in previous computational

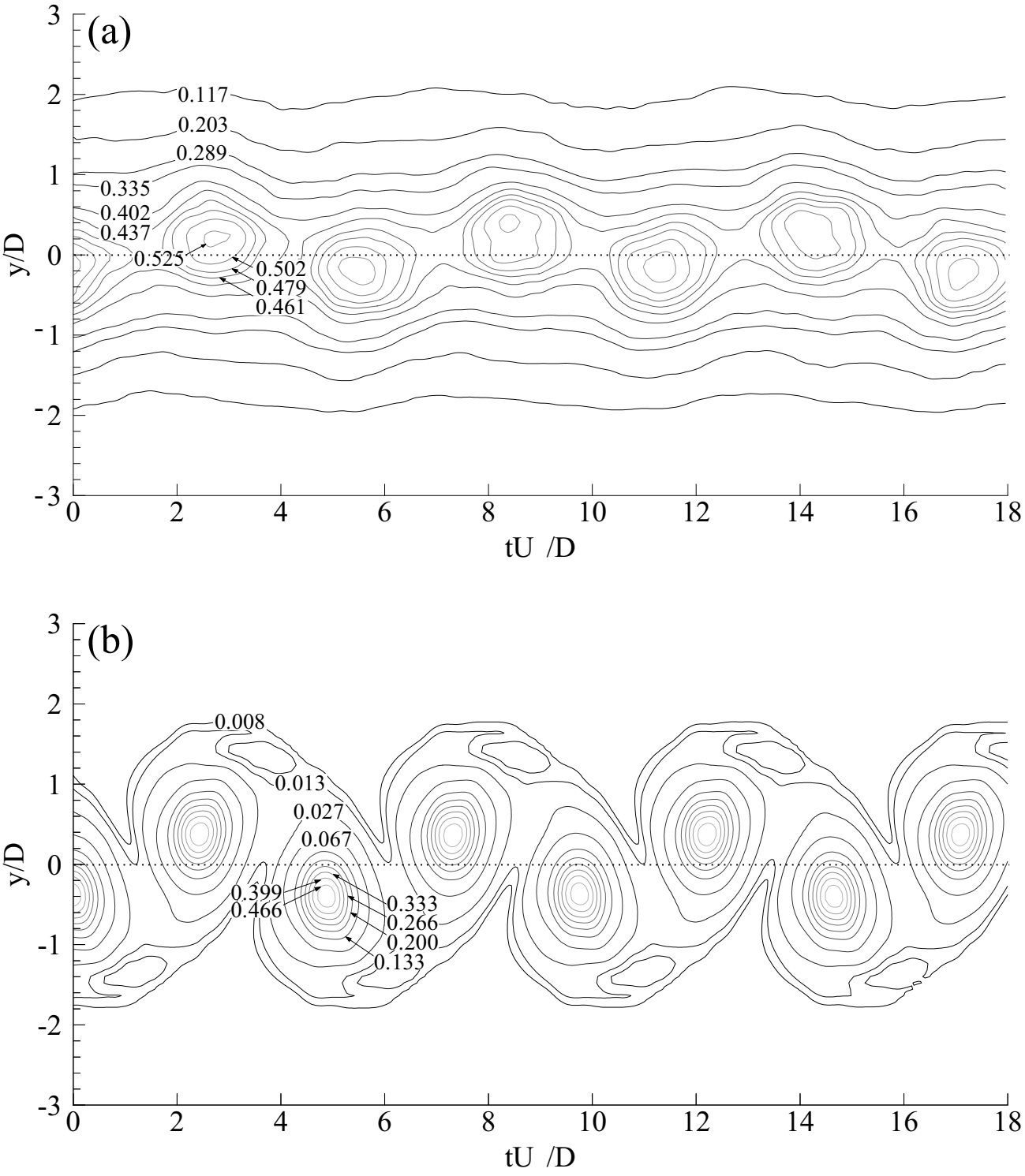

Fig. 7 Normalised entropy contours. (a) **Experiment,** (b) **Numerical prediction.**

work[8,9] to be a predominant source of entropy production in the near wake region. The influence of the shearing flow is still identifiable to a lesser degree in the numerical prediction at the current downstream position of six cylinder diameters, Fig 7(b).

CONCLUDING REMARKS

The energy separation characteristics downstream of a circular cylinder in compressible flow have been investigated through comparison of a time accurate experimental program with a time dependent numerical model. Periodic vortex shedding is observed in both the measured and predicted results downstream of the circular cylinder at Mach 0.6. These form the familiar von Kármán vortex street. Redistribution of the total temperature and total pressure occurs in the vortex street. 'Hot spots' of increased total temperature are located at the edge of the wake and 'cold spots' of decreased total temperature are located close to the wake centre. The non-uniform total temperature and total pressure distribution downstream of the cylinder is a source of entropy production. Good agreement in the magnitude of the total temperature at the hot and cold spots is observed in the measured and predicted results. The hot and cold spots are close in normalised amplitude to published results from a similar prediction of the energy separation downstream of a circular cylinder at Mach 0.35. The time averaged result of the non-uniform total temperature distribution is the Eckert-Weise effect. The time accurate measurements highlight the versatility of the total temperature wake probes developed by Buttsworth and Jones.[17]

Comparison of the experimental measurements with the numerical prediction has highlighted the influence of the boundary layer development and separation on the vortex shedding characteristics and, therefore, on the magnitude and location of the non-uniform total temperature and total pressure distribution downstream of the circular cylinder. This comparison emphasizes the importance of including the effects of turbulence and boundary layer development in the numerical study of this predominantly inviscid flow phenomenon. The comparison of the measured results with the prediction emphasizes the advantage of an integrated experimental and numerical flow field study.

In highly loaded turbomachinery, the entropy production associated with the total temperature and pressure redistribution can lead to a reduction in stage performance.[6,7] Any prediction of the flow around turbomachinery blading with thick trailing edges therefore needs to consider the physics of energy separation.

ACKNOWLEDGEMENTS

This work is carried out under grateful acknowledgement of a research grant from the British EPSRC. The authors wish to acknowledge J. Templin of the National Research Council of Canada for the use of the U-66 wind tunnel and workshop facilities. In addition thanks are due to Prof. T.V. Jones, Dr S.I. Hogg, Mr P. Hunt and Dr E. Hanff.

REFERENCES

[1]Eckert, E. R. G. and Weise, W., *Forschg. Ing. Wesen.*, Vol. 13, 1943, pp. 246–254.

[2]Ryan, L., "Experiments on aerodynamic cooling," Tech. Rep. 18, ETH Inst. für Aerodynamik Mitteilungen, 1951.

[3]Thomann, H., "Measurements of the recovery temperature in the wake of a cylinder and of a wedge at Mach numbers between 0.5 and 3," FFA Report 84, Flygtekniska Försöksanstalten (The Aeronautical Research Institute of Sweden), Stockholm, Sweden, June 1959.

[4]Kurosaka, M., Gertz, J. B., Graham, J. E., Goodman, J. R., Sundaram, P., Riner, W. C., Kuroda, H., and Hankey, W. L., "Energy separation in a vortex street," *J. Fluid Mechanics*, Vol. 178, May 1987, pp. 1–29.

[5]Carscallen, W. E. and Oosthuizen, P. H., "The effect of secondary flow on the redistribution of the total temperature field downstream of a stationary turbine cascade," CP 469, AGARD, 1989.

[6]Carscallen, W. E., Hogg, S. I., Gostelow, J. P., and Buttsworth, D.R., "Time resolved measurements of the energy separation process in a transonic turbine vane wake flow," AGARD Advanced Aerodynamic Measurement Technology Meeting, Seattle, Paper no. 16, September 1997.

[7]Carscallen, W. E., Currie, T. C., Hogg, S. I., and Gostelow, J. P., "Measurements and computation of energy separation in the vortical wake flow of a turbine nozzle cascade," Paper 98-GT-477, ASME, June 1998.

[8]Rona, A. and Bennett, W.P., "Energy separation in a compressible vortex street," Paper 2001-0601, AIAA, Jan. 2001.

[9]Rona, A. and Bennett, W.P., "Non-uniform total temperature in a turbulent vortex street," Paper 2001-2467, AIAA, June. 2001.

[10]Lilley, G., Zhang, X., and Rona, A., "Progress in computational aeroacoustics in predicting the noise radiated from turbulent flows," *Int. J. Acous. and Vib.*, Vol. 2, No. 1, May 1997, pp. 2–9.

[11]Wilcox, D., *Turbulence modelling for CFD*, Griffin Printing, Glendale, California, USA, 1993.

[12]Roe, P. L., "Approximate Riemman solvers, parameter vectors, and difference schemes," *J. Comp. Physics*, Vol. 43, 1981, pp. 357–372.

[13]Roe, P. L., "Some contributions to the modelling of discontinuous flows," Lectures in Applied Math. 22, Am. Math. Soc., 1985.

[14]Hu, F. Q., Hussaini, M. Y., and Manthey, J., "Application of low dissipation and dispersion Runge-Kutta schemes to benchmark problems in computational aeroacoustics," *ICASE/LaRC workshop on benchmark problems in computational aeroacoustics (CAA)*, edited by J. C. Hardin, J. R. Ristorcelli, and C. K. W. Tam, NASA Conference Publication 3300, May 1995, pp. 73–98.

[15]Hoffman, K. A. and Chiang, S. T., *Computational fluid dynamics for engineers*, Vol. 1, Engineering Education System, Wichita, USA, 3rd ed., March 1995.

[16]Giles, M. B., "Nonreflecting boundary conditions for Euler equations calculations," *AIAA J.*, Vol. 18, No. 12, 1990, pp. 2050–2058.

[17]Buttsworth, D.R., and Jones, T.V., "A fast response total temperature probe for unsteady compressible flows," *AMSE*

J. Engineering for Gas Turbines and Power, Vol. 120, 1996, pp. 694–701.

[18]Oldfield, M.L.G., Burd, H.J., and Doe, N.G., "Design of wide-bandwidth analogue circuits for heat transfer instrumentation in transient tunnels," 16^{th} Symposium of International Centre for Heat and Mass Transfer, Hemisphere Publishing, 1982, pp. 233–257.

[19]Douglas, J., Gasiorek, J., and Swaffield., J., *Fluid Mechanics*, Longman, Harlow, England, 3rd ed., 1995.